

Wind Profile and Drag Coefficient over Mature Ocean Surface Wave Spectra

TETSU HARA

Graduate School of Oceanography, University of Rhode Island, Narragansett, Rhode Island

STEPHEN E. BELCHER

Department of Meteorology, University of Reading, Reading, United Kingdom

(Manuscript received 4 March 2003, in final form 30 March 2004)

ABSTRACT

The mean wind profile and the Charnock coefficient, or drag coefficient, over mature seas are investigated. A model of the wave boundary layer, which consists of the lowest part of the atmospheric boundary layer that is influenced by surface waves, is developed based on the conservation of momentum and energy. Energy conservation is cast as a bulk constraint, integrated across the depth of the wave boundary layer, and the turbulence closure is achieved by parameterizing the dissipation rate of turbulent kinetic energy. Momentum conservation is accounted for by using the analytical model of the equilibrium surface wave spectra developed by Hara and Belcher. This approach allows analytical expressions of the Charnock coefficient to be obtained and the results to be examined in terms of key nondimensional parameters. In particular, simple expressions are obtained in the asymptotic limit at which effects of viscosity and surface tension are small and the majority of the stress is supported by wave drag. This analytical model allows us to identify the conditions necessary for the Charnock coefficient to be a true constant, an assumption routinely made in existing bulk parameterizations.

1. Introduction

Present parameterizations of the wind stress, or equivalently the drag coefficient, over the ocean are far from satisfactory, as pointed out in the recent book by Jones and Toba (2001). Most operational atmospheric models use a simple bulk parameterization based on the equivalent surface roughness z_0 being determined by

$$\frac{gz_0}{u_*^2} = \text{const} \quad (1)$$

(Charnock 1955), where g is gravitational acceleration and u_* is the wind friction velocity. This constant is called the Charnock coefficient and is usually set to be about 0.010–0.015. It is still being debated whether the Charnock coefficient is a true constant or depends on the wind stress and other parameters (e.g., Yelland and Taylor 1996; Donelan et al. 1997; Taylor and Yelland 2001). One of the main uncertainties regarding the drag coefficient estimation is the effect of the ocean surface wave field. The bulk formulation is expected to be valid only over a fully developed wave field. The effect of growing or confused seas is still difficult to predict. Jones and Toba (2001) review previous studies of the

effect of the inverse wave age (u_*/c_p) on the Charnock coefficient (here c_p is the phase speed of dominant waves) and conclude that the results are still far from conclusive.

There have been many attempts to predict the drag coefficient by explicitly calculating the stress supported by surface waves, the so-called wave-induced stress. Over the ocean surface, in stationary homogeneous conditions the total stress is independent of height in the lower part of the atmospheric boundary layer, the constant stress layer. Since the total stress is the sum of the turbulent stress and the wave-induced stress (except inside the viscous sublayer), the turbulent stress is reduced inside the wave boundary layer. Earlier studies employed an eddy viscosity model to relate the reduced turbulent stress to the mean wind profile (Janssen 1989; Chalikov and Makin 1991; Makin et al. 1995) and then predict the drag coefficient. Makin and Kudryavtsev (1999) proposed a modified expression of the eddy viscosity based on the turbulent kinetic energy budget inside the wave boundary layer. All of these studies used empirical parameterizations of the surface wave field. More recently, Kudryavtsev and Makin (2001) introduced a much simplified model of the wave boundary layer and included the effect of airflow separation due to surface breaking waves. They also used the model for the surface wave spectrum of Kudryavtsev et al. (1999) instead of using an empirical surface wave spec-

Corresponding author address: Dr. Tetsu Hara, Graduate School of Oceanography, University of Rhode Island, South Ferry Road, Narragansett, RI 02882.
E-mail: thara@uri.edu

trum. Makin and Kudryavtsev (2002) further included the effect of dominant wave breaking to the model of Kudryavtsev and Makin (2001).

What these studies all show is that it is the short waves in the wave spectrum (say, less than 10 m in wavelength) that dominate the roughness of the sea surface and hence the drag. This part of the spectrum is often in a local equilibrium. Recently, Hara and Belcher (2002) developed a simple analytical model of this equilibrium range of surface gravity wave spectra. The model predicts that the equilibrium surface wave spectrum is determined by a single parameter k_s , called a sheltering wavenumber. The sheltering wavenumber is determined by how the total wind stress is partitioned into stress supported by different parts of the wave spectrum as well as the surface viscous stress. Here we use this analytical model of the equilibrium wave spectrum to calculate the Charnock coefficient and mean wind profile over mature seas. The study draws from the approach of Makin and Mastenbroek (1996) and Makin and Kudryavtsev (1999), in that it is based on conservation of momentum and energy in the wave boundary layer, but there are important differences:

- 1) Energy conservation is cast as a bulk constraint, integrated across the depth of the wave boundary layer, which demonstrates that it is natural and sufficient to close the turbulence by parameterizing the dissipation rate of turbulent kinetic energy.
- 2) Momentum conservation is accounted for using the analytical model developed by Hara and Belcher (2002). This allows us to obtain analytical expressions of the Charnock coefficient, and to examine the results in terms of key nondimensional parameters.

As in Makin and Kudryavtsev (1999), we assume that surface waves are not breaking and the airflow remains attached to the water surface with a viscous sublayer established just above the water surface.

In section 2 we briefly review the model of the equilibrium wave spectrum by Hara and Belcher (2002) and estimate the sheltering wavenumber k_s over mature seas in section 3. A new model of the wave boundary layer is introduced in section 4 and the mean wind profile and the Charnock coefficient over mature seas are calculated, followed by concluding remarks in section 5.

2. Theory of equilibrium wave spectrum

In this section, we briefly review the theoretical model of the equilibrium range of surface wave spectra developed by Hara and Belcher (2002). The model starts with the conservation of momentum inside the wave boundary layer. The mean wind and the wave field are assumed to be aligned. The total air-sea momentum flux τ_{tot} is expressed as a sum of the wave-induced stress $\tau_w(z)$ and the turbulent stress $\tau_t(z)$,

$$\tau_{\text{tot}} = \rho_a u_*^2 = \tau_w(z) + \tau_t(z), \quad (2)$$

where ρ_a is air density, u_* is the friction velocity, and z is the height above the instantaneous water surface [see Makin et al. (1995) and Makin and Kudryavtsev (1999) for discussion of the wave-following coordinate]. The wave-induced stress is expressed as

$$\tau_w(z) = \int_0^\infty \int_{-\pi/2}^{\pi/2} \beta_g(k, \theta) \rho_w \sigma B(k, \theta) \times k^{-4} F(k, z) \cos \theta d\theta dk. \quad (3)$$

(The contribution to the wave-induced stress from waves propagating against the wind, i.e., $|\theta| > \pi/2$, is negligible because the energy in these components is so small. Therefore, the integration in θ spans $-\pi/2$ to $\pi/2$ only.) Here β_g is the wave growth rate, ρ_w is water density, k is the wavenumber, σ is the wave angular frequency, θ is the wave propagation direction relative to the mean wind direction, and B is the degree of saturation, which is related to the wave height spectrum ψ as $B = k^4 \psi$. Following Makin et al. (1995), the decay function $F(k, z)$ is approximated by a step function, namely,

$$\begin{aligned} F(k, z) &= 1, & z \leq L(k), & \text{and} \\ F(k, z) &= 0, & z > L(k). \end{aligned} \quad (4)$$

Following Belcher and Hunt (1993) the wave-induced stress penetrates a distance $L(k)$ into the airflow and so we set $kL(k) = \delta = \text{const}$. The wave-induced stress then becomes

$$\tau_w(z) = \int_0^{\delta/z} \int_{-\pi/2}^{\pi/2} \beta_g(k, \theta) \rho_w \sigma B(k, \theta) k^{-4} \cos \theta d\theta dk; \quad (5)$$

that is, it is equal to the total momentum flux into surface waves in the wavenumber range of $0 < k < \delta/z$. If we interpret height $L(k)$ as a blending height, then δ is a constant $O(0.05)$ (Mason 1988).

Belcher (1999) and Makin and Kudryavtsev (1999) show that the growth rate $\beta_g(k, \theta)$ of a particular wave scale is determined by the turbulent stress τ_t evaluated at the height comparable to the depth of the inner region $L(k)$; that is,

$$\begin{aligned} \tau_t[z = L(k)] &= \tau_{\text{tot}} - \tau_w[z = L(k)] \\ &= \tau_{\text{tot}} - \int_0^k \int_{-\pi/2}^{\pi/2} \beta_g(k', \theta) \rho_w \sigma B(k', \theta) \\ &\quad \times k'^{-4} \cos \theta d\theta k' dk'. \end{aligned} \quad (6)$$

This is called a local turbulent stress and is denoted by $\tau_t^l(k) = \rho_a [u_*^l(k)]^2$. It is seen from (6) that the local turbulent stress, which forces waves of a wavenumber k , is equal to the total wind stress minus the stress supported by all the longer waves. Then, the growth rate is described by

$$\beta_g(k, \theta) = c_\beta \sigma \frac{\rho_a [u_*^l(k)]^2}{\rho_w c^2} h(\theta) \quad \left[\frac{u_*^l(k)}{c} \geq \alpha_2 \right]$$

and

$$\beta_g(k, \theta) = 0 \quad \left[\frac{u_*^l(k)}{c} < \alpha_2 \right], \quad (7)$$

where c_β is an empirical coefficient and $h(\theta)$ is the directionality of the wave growth rate. The coefficient α_2 , which defines the smallest wavenumbers that are forced by the wind, is set to 0.07 after Plant (1982).

The evolution of the surface wave spectrum is described in terms of the wave action spectral density $N(\mathbf{k})$,

$$\frac{dN}{dt} = -\nabla_{\mathbf{k}} \cdot T(\mathbf{k}) + S_w - D, \quad (8)$$

where \mathbf{k} is the wavenumber vector, $T(\mathbf{k})$ is the flux of the wave action by nonlinear wave interactions, $\nabla_{\mathbf{k}}$ is the gradient operator in \mathbf{k} , S_w is the wind input, and D is the dissipation. The action density is related to the wave height spectrum $\psi(\mathbf{k})$ and the degree of saturation $B(\mathbf{k})$ as

$$N(\mathbf{k}) = g^{1/2} k^{-1/2} \psi(\mathbf{k}) = g^{1/2} k^{-9/2} B(\mathbf{k}), \quad k = |\mathbf{k}| \quad (9)$$

for surface gravity waves, where g is the gravitational acceleration. It is well known that ocean surface wave spectra at frequencies much higher than the peak frequency attain an equilibrium state (called an ‘‘equilibrium range’’; e.g., Phillips 1977). In the equilibrium range, the three input terms to the wave action conservation equation balance one another to achieve a quasi steady state (Phillips 1985); that is, the right-hand side of (8) is equal to zero.

As in Phillips (1985), Hara and Belcher (2002) assume that both the divergence of the wave action flux $\nabla_{\mathbf{k}} \cdot T(\mathbf{k})$ and the dissipation D in the wave action equation are proportional to the cube of the local wavenumber spectrum. Since the sum of these two terms is balanced by the input term in the equilibrium range, we may set

$$\nabla_{\mathbf{k}} \cdot T(\mathbf{k}) + D = S_w = \alpha g k^{-4} B^3(\mathbf{k}), \quad (10)$$

where α is a nondimensional proportionality constant. The wind input term is expressed as

$$S_w = \beta_g(\mathbf{k}) N(\mathbf{k}) = \beta_g(\mathbf{k}) g^{1/2} k^{-9/2} B(\mathbf{k}), \quad (11)$$

where $\beta_g(\mathbf{k})$ is the wave growth rate described in (7). Introducing (11) into (10), the degree of saturation is expressed in terms of the growth rate as

$$B(\mathbf{k}) = [\alpha^{-1} \beta_g(\mathbf{k}) g^{-1/2} k^{-1/2}]^{1/2}. \quad (12)$$

On differentiating (6) by k and introducing (12) and (7), we obtain an integral equation of u_*^l , which can be solved analytically provided proper boundary conditions are specified. Let the equilibrium range be established for a wavenumber range of $k_0 < k < k_1$ and let us specify the local friction velocities at k_0 and k_1 , de-

noted by u_{*0} and u_{*1} , respectively. Then, the solution for the local friction velocity is written

$$u_*^l(k) = \frac{2u_{*s}}{1 + (k/k_s)^{1/2}}, \quad (13)$$

where

$$k_s = \left(\frac{-k_0^{1/2} u_{*0} + k_1^{1/2} u_{*1}}{u_{*0} - u_{*1}} \right)^2 \quad (14)$$

is called a sheltering wavenumber and

$$u_{*s} = \frac{(k_1^{1/2} - k_0^{1/2}) u_{*1} u_{*0}}{2(k_1^{1/2} u_{*1} - k_0^{1/2} u_{*0})} \quad (15)$$

is called a sheltering friction velocity. The sheltering wavenumber k_s represents the wavenumber at which the local friction velocity begins to be affected by sheltering by the longer wavelength waves. At low wavenumbers ($k \ll k_s$), u_*^l becomes constant and equal to $2u_{*s}$, while u_*^l decreases like $k^{-1/2}$ at high wavenumbers ($k \gg k_s$). If the solution (13) is introduced back into the differential equation for u_*^l , the coefficient α is found to be

$$\alpha = 4 \frac{\rho_a}{\rho_w} c_\beta^3 c_\theta^2 \left(\frac{u_{*s}}{c_s} \right)^2, \quad (16)$$

where $c_s = (g/k_s)^{1/2}$ is called a sheltering wave phase speed, c_s/u_{*s} is called a sheltering wave age, and

$$c_\theta = \int_{-\pi/2}^{\pi/2} [h(\theta)]^{3/2} \cos \theta \, d\theta. \quad (17)$$

Introducing (11), (13), and (16) into (12), the degree of saturation B is found to be

$$B(k, \theta) = \frac{1}{c_\beta c_\theta} \left[1 + \left(\frac{k_s}{k} \right)^{1/2} \right]^{-1} h(\theta)^{1/2}. \quad (18)$$

If integrated over all angles, the solution becomes

$$B(k) = \frac{1}{c_\beta c_\theta'} \left[1 + \left(\frac{k_s}{k} \right)^{1/2} \right]^{-1}, \quad (19)$$

with

$$\begin{aligned} \frac{1}{c_\theta'} &= \frac{1}{c_\theta} \int_{-\pi/2}^{\pi/2} h(\theta)^{1/2} \, d\theta \\ &= \frac{\int_{-\pi/2}^{\pi/2} h(\theta)^{1/2} \, d\theta}{\int_{-\pi/2}^{\pi/2} h(\theta)^{3/2} \cos \theta \, d\theta}. \end{aligned} \quad (20)$$

At low wavenumbers ($k \ll k_s$), where the sheltering effect is weak, $B(k)$ is proportional to $k^{1/2}$ and is consistent with the prediction by Phillips (1985). At high wavenumbers ($k \gg k_s$), $B(k)$ is strongly influenced by the sheltering effect and becomes independent of wave-

number. Last, using the linear dispersion relation, the frequency spectrum is obtained from (19), namely,

$$\Phi(\sigma) = \frac{2}{c_\beta c'_\theta} g^2 \sigma^{-5} \left[1 + \left(\frac{\sigma_s}{\sigma} \right) \right]^{-1}, \quad (21)$$

where $\sigma_s = (gk_s)^{1/2}$. Therefore, the frequency spectrum is proportional to σ^{-4} at low frequencies ($\sigma \ll \sigma_s$) and is proportional to σ^{-5} at high frequencies ($\sigma \gg \sigma_s$).

In summary, the equilibrium spectrum is determined by two empirical coefficients, c_β and c'_θ , and a single dynamical variable, k_s , called a sheltering wavenumber. In the next section we estimate the value of k_s for mature seas.

3. Calculation of the sheltering wavenumber for mature seas

In this section we present two different approaches to determine the sheltering wavenumber k_s over mature seas. The first approach is based on measured values of the stress and is the same as the method used by Hara and Belcher (2002); the second is based on comparison with the measured wave spectra.

a. Approach I

Hara and Belcher (2002) calculate the sheltering wavenumber k_s for mature seas using the empirical observations of the total wind stress ($\rho_a u_{*0}^2$) and the surface viscous stress ($\rho_a u_{*v}^2$) provided by Banner and Peirson (1998). They start with two assumptions:

- 1) The lower bound of the equilibrium range is set:

$$k_0 = \frac{\alpha_2^2 g}{u_{*0}^2} \quad \text{or} \quad \frac{u_{*0}}{c_0} = \alpha_2 \quad (22)$$

with $c_0 = (g/k_0)^{1/2}$, and $\alpha_2 = 0.07$, because wind forcing is negligible below this wavenumber according to Plant (1982). Then the local stress, $\rho_a u_{*0}^2$, evaluated at k_0 is equal to the total stress, $\rho_a u_{*v}^2$.

- 2) The upper bound of the equilibrium range is $k_1 = 100 \text{ rad m}^{-1}$ and the local stress, $\rho_a u_{*1}^2$, evaluated at k_1 is equal to the viscous stress, $\rho_a u_{*v}^2$, at the surface.

They then use Banner and Peirson's (1998) estimates of u_{*0} and u_{*v} to calculate the upper and lower bounds of k_s . The results are reproduced in Fig. 1. The estimated value of k_s monotonically decreases as u_{*0} increases.

b. Approach II

An alternative approach to estimate k_s is to use the observed equilibrium wave spectra. Phillips (1985) shows that previous observational data of the equilibrium frequency spectrum agree with his predicted form,

$$\Phi(\sigma) = \alpha_p g u_{*0} \sigma^{-4}, \quad (23)$$

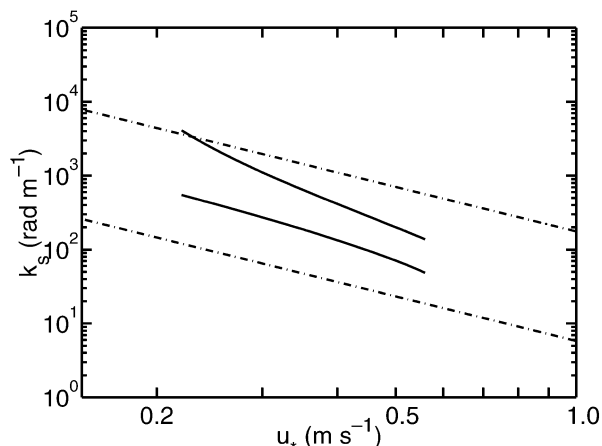


FIG. 1. Upper and lower bounds of sheltering wavenumbers k_s vs wind friction velocity u_{*0} for mature seas. Solid lines indicate estimates based on approach I with data of Banner and Peirson (1998). Dash-dot lines indicate estimates based on approach II with the data collated by Phillips (1985) with sheltering wave age $c_s/u_{*0} = 0.46$ and 2.38.

for frequencies not too far from the peak and that the empirical constant α_p is between 0.02 and 0.11 (and between 0.06 and 0.11 for most of the field observations). Our model, on the other hand, yields

$$\Phi(\sigma) = \frac{2}{c_\beta c'_\theta} g^2 \sigma^{-4} \sigma_s^{-1} = \frac{2}{c_\beta c'_\theta} \left(\frac{g}{k_s u_{*0}^2} \right)^{1/2} g u_{*0} \sigma^{-4}, \quad (24)$$

for $\sigma \ll \sigma_s$, which is a good approximation not far from the spectral peak. Equating (23) and (24), we may write the sheltering wavenumber in terms of α_p :

$$k_s = \frac{g}{u_{*0}^2} \left(\frac{1}{2} c_\beta c'_\theta \alpha_p \right)^{-2} \quad \text{or} \quad \frac{c_s}{u_{*0}} = \frac{1}{2} c_\beta c'_\theta \alpha_p. \quad (25)$$

Therefore, k_s is proportional to u_{*0}^{-2} and is determined by three empirical coefficients, c_β , c'_θ , and α_p . This estimate of k_s is also shown in Fig. 1 for $\alpha_p = 0.02$ and 0.11. Here, we have set $c_\beta = 40$, following Plant (1982), and $c'_\theta = (3/16)\pi$ corresponding to $h(\theta) = \cos^2 \theta$. For a fixed u_{*0} , this estimate yields a relatively wide range of k_s , which includes the range of k_s estimated from approach I.

It is noteworthy that, if we set $k = k_0$ and $u_{*0}^l(k) = u_{*0}$ in (13) and introduce (22), we obtain

$$\frac{2u_{*0}}{u_{*0}} = 1 + \alpha_2 \frac{c_s}{u_{*0}}. \quad (26)$$

Therefore, we can write the sheltering wave age as

$$\frac{c_s}{u_{*0}} = 2 \frac{c_s}{u_{*0}} \left(1 + \alpha_2 \frac{c_s}{u_{*0}} \right)^{-1}. \quad (27)$$

Now, if the Phillips (1985) constant, α_p , is truly constant and independent of u_{*0} , then (25) shows that c_s/u_{*0} is also constant, and so according to (27) the sheltering wave age c_s/u_{*0} is also independent of u_{*0} . Since the

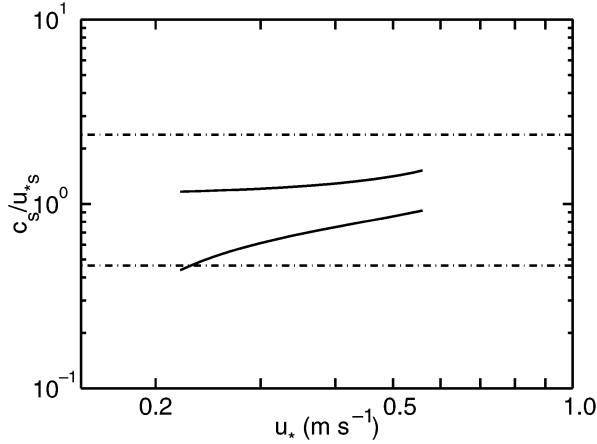


FIG. 2. Upper and lower bounds of sheltering wave age c_s/u_{*s} vs wind friction velocity u_* for mature seas. Solid lines indicate estimates based on approach I with data of Banner and Peirson (1998). Dash-dot lines indicate estimates based on approach II with the data collated by Phillips (1985) with sheltering wave age $c_s/u_{*s} = 0.46$ and 2.38.

sheltering wave age is related to α through (16), the proportionality constant α , originally defined in (10), is then also a constant. The lower and upper bounds of the sheltering wave age, corresponding to $\alpha_p = 0.02$ and 0.11, are $c_s/u_{*s} = 0.46$ and 2.38. In contrast, the sheltering wavenumber estimated from approach I yields the sheltering wave age that depends weakly on u_* . Figure 2 shows the variation of sheltering wave age calculated using these two methods.

4. Effect of mature seas on the atmospheric wave boundary layer

In this section, we first develop a model of the wave boundary layer based on the conservation of momentum (described in section 2) and energy (section 4a). Next, the equilibrium spectral model of Hara and Belcher (2002), described in section 2, and the estimates of the sheltering wave age c_s/u_{*s} , described in section 3, are introduced into the model to calculate the Charnock coefficient (sections 4b–4d) and the mean wind profile (section 4e) over mature seas. Throughout this study the wave field is assumed to be aligned with the mean wind direction.

a. Conservation of energy in the wave boundary layer

Previously, the effect of surface waves on the mean wind profile was estimated using eddy viscosity models (Janssen 1989; Chalikov and Makin 1991; Makin et al. 1995; Makin and Kudryavtsev 1999). It can be shown that these models do not conserve energy within the wave boundary layer (see appendix A). Makin and Mastenbroek (1996) introduced a wave boundary layer model that does satisfy both momentum conservation and

energy conservation. Here, we develop a simple model of the wave boundary layer based on bulk conservation of energy, which demonstrates that it is natural and sufficient to effect turbulence closure by parameterizing the dissipation rate of the turbulent kinetic energy (TKE).

Let us introduce a coordinate system in a fixed frame of reference (in horizontal) and define the positive x direction as the mean wind direction. The z coordinate is the height above the instantaneous water surface as defined earlier. We then introduce the following decomposition of the wind velocity u_i ($i = 1, 2, 3$) and pressure p ,

$$u_i = \bar{u}_i + \tilde{u}_i + u'_i \quad \text{and} \quad p = \bar{p} + \tilde{p} + p', \quad (28)$$

where the overbar denotes time average, the tilde denotes the wave-correlated part of the signal, and the prime denotes the turbulent fluctuation. The total kinetic energy is also decomposed into

$$e = \frac{1}{2} u_i u_i = \bar{e} + \tilde{e} + e', \quad (29)$$

and the mean kinetic energy \bar{e} itself consists of three components,

$$\bar{e} = \frac{1}{2} \bar{u}_i \bar{u}_i + \frac{1}{2} \overline{\tilde{u}_i \tilde{u}_i} + \frac{1}{2} \overline{u'_i u'_i}. \quad (30)$$

The turbulent and wave-induced stresses are written as

$$\tau_i = -\rho_a \overline{u' w'} \quad \text{and} \quad \tau_w = -\rho_a \overline{\tilde{u} \tilde{w}}. \quad (31)$$

Following Makin and Mastenbroek (1996), the energy budget for the airflow over surface waves can be expressed as the budget for each of the three components of the mean kinetic energy. The budget of the mean kinetic energy of mean motions, $\frac{1}{2} \bar{u}^2$, is

$$\frac{d}{dz} (\bar{u} \tau_{\text{tot}}) - P^t - D^w = 0; \quad (32)$$

the budget of the mean kinetic energy of wave-induced motions, $\frac{1}{2} \overline{\tilde{u}_i \tilde{u}_i}$, is

$$\frac{d\Pi}{dz} + D^w - P^w = 0; \quad (33)$$

and the budget for the mean TKE, $\frac{1}{2} \overline{u'_i u'_i}$, is

$$\frac{d\Pi'}{dz} + (P^t + P^w) - \rho_a \varepsilon = 0. \quad (34)$$

Here, $P^t = \tau_i d\bar{u}/dz$ is production of the TKE from the mean velocity shear;

$$P^w = -\rho_a \overline{(u'_i u'_j) \frac{\partial \tilde{u}_i}{\partial x_j}} \quad (35)$$

is production of the TKE from work done by wave-induced turbulent stress against wave-induced shear; $D^w = \tau_w d\bar{u}/dz$ is transfer of energy from the mean to the wave-induced motions;

$$\Pi = -\overline{w\bar{p}} - \overline{\rho_a \tilde{u}_i (\tilde{u}'_i w')} \quad (36)$$

is the vertical transport of the kinetic energy of the wave-induced motions;

$$\Pi' = -\overline{w'p'} - \frac{\rho_a}{2} \overline{w'(\tilde{u}'_i \tilde{u}'_i)} - \frac{\rho_a}{2} \overline{w'u'_i u'_i} \quad (37)$$

is the vertical transport of the TKE; and ε is the viscous dissipation of the TKE. The total energy budget is obtained by adding (32) to (34),

$$\frac{d}{dz}(\bar{u}\tau_{\text{tot}}) + \frac{d\Pi}{dz} + \frac{d\Pi'}{dz} - \rho_a \varepsilon = 0, \quad (38)$$

which states that the difference between the shear production and the viscous dissipation is balanced by the divergence of the total energy flux ($\Pi + \Pi'$). Therefore, inside the wave boundary layer the shear production is not equal to the viscous dissipation. Above the top of the wave boundary layer Π and Π' are both negligibly small and the shear production balances the viscous dissipation.

At the ocean surface the largest contribution to the vertical transport of the wave-induced energy is from the pressure transport,

$$\Pi(z=0) = -\overline{w\bar{p}}, \quad (39)$$

because at the ocean surface $-\overline{w\bar{p}}$ is equal to the energy flux into surface waves. (The contribution to Π from the surface shear stress is negligible for surface gravity waves.) Hence, we may write

$$\Pi(z=0) = \int_0^\infty \tilde{F}_w(k) dk \quad (40)$$

with

$$\tilde{F}_w(k) = \int_{-\pi/2}^{\pi/2} \beta_g(k, \theta) \rho_w g B(k, \theta) k^{-3} d\theta. \quad (41)$$

The lower boundary condition on the mean wind speed is given in terms of the equivalent roughness scale z_v of the viscous sublayer,

$$\bar{u} = 0 \quad \text{at } z = z_v = 0.1 \frac{\nu_a}{u_{*v}}, \quad (42)$$

where ν_a is the air viscosity and $\rho_a u_{*v}^2$ is the surface viscous stress. If we integrate (38) from $z = z_v$ to the top of the wave boundary layer ($z = z_T$), we obtain the equation for *bulk conservation of energy*:

$$\tau_{\text{tot}} \bar{u}(z_T) - \Pi(0) - \rho_a \int_{z_v}^{z_T} \varepsilon dz = 0 \quad (43)$$

since $\Pi(z_T) = 0$ and $\Pi(z_v) = \Pi(0)$.

As schematically shown in Fig. 3, the bulk energy conservation requires that the total energy flux from the top must be equal to the sum of the energy flux into surface waves and the total viscous dissipation of the

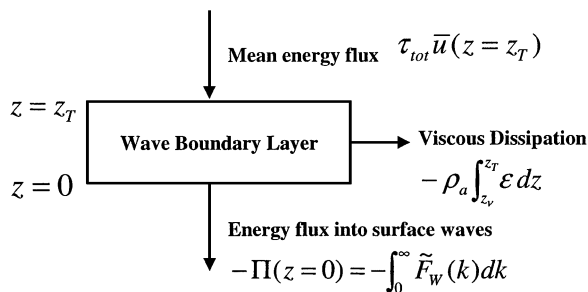


FIG. 3. Schematic of energy conservation inside wave boundary layer.

TKE inside the wave boundary layer. Above the wave boundary layer, the mean velocity profile becomes a standard logarithmic layer, with a roughness length that characterizes the sea surface. Thus, from the condition of bulk conservation of energy, once the total stress, the total energy flux into waves, and the total TKE viscous dissipation in the wave boundary layer are known, we may determine $\bar{u}(z_T)$ and hence the equivalent roughness length and the drag coefficient. This demonstrates that it is natural and sufficient to close the turbulence by parameterizing the dissipation rate of turbulent kinetic energy. Therefore, we do not introduce eddy viscosity and prognostic equations for turbulence closure as in Makin and Mastenbroek (1996). Instead, following the approach used in one-equation models of turbulence, the viscous dissipation of the TKE, ε , is simply related to the local turbulent stress, u_*^l , at each height (rather than the total stress) so that

$$\varepsilon(z) = \frac{[u_*^l(k = \delta/z)]^3}{\kappa z}, \quad (44)$$

where κ is the von Kármán constant.

b. Analytical expression of the equivalent roughness over mature seas

Consider now a fully grown sea with the equilibrium spectral form presented in section 2. As before, the wavenumber k_0 is set to the lower bound of the equilibrium range such that $u_*^l/c_0 = \alpha_2 = 0.07$. We also set $u_*^l(k_0) = u_*$; that is, the wave growth rate is zero for $k < k_0$. In addition, the equilibrium spectrum obtained from section 3 is valid up to the large wavenumber cutoff k_1 , which thus neglects effects of surface tension and viscosity on waves up to k_1 . Last, assume that there are no waves for $k > k_1$ so that $u_{*1} = u_{*v}$. The flux into surface waves $\tilde{F}_w(k)$ is evaluated using the definition of the growth rate β_g in (7), as well as the equilibrium form of $B(k)$, given in (18), and u_*^l , given in (13). This procedure yields

$$\tilde{F}_w(k) = \rho_a u_*^3 c_\theta'' \frac{c_s}{u_{*s}} \left[\frac{u_*^l(k)}{u_*} \right]^3 \frac{1}{k} \quad (45)$$

with

$$c_\theta'' = \frac{1}{2c_\theta} \int_{-\pi/2}^{\pi/2} [h(\theta)]^{3/2} d\theta. \quad (46)$$

Introducing (44) and (45) into (43), the mean wind speed at the top of the wave boundary layer ($z = z_\tau = \delta/k_0$) is found to be

$$\frac{\kappa \bar{u}(z = \delta/k_0)}{u_*} = \int_{k_0}^{k_1} \kappa c_\theta'' \frac{c_s}{u_{*s}} \left[\frac{u_*'(k)}{u_*} \right]^3 \frac{dk}{k} + \int_{z_\nu}^{\delta/k_1} \left(\frac{u_{*1}}{u_*} \right)^3 \frac{dz}{z} + \int_{\delta/k_1}^{\delta/k_0} \left[\frac{u_*'(k = \delta/z)}{u_*} \right]^3 \frac{dz}{z} \quad (47)$$

$$= \left(\kappa c_\theta'' \frac{c_s}{u_{*s}} + 1 \right) \int_{k_0}^{k_1} \left[\frac{u_*'(k)}{u_*} \right]^3 \frac{dk}{k} + \int_{z_\nu}^{\delta/k_1} \left(\frac{u_{*1}}{u_*} \right)^3 \frac{dz}{z}, \quad (48)$$

which can be integrated (see appendix B for derivation) to yield

$$\frac{\kappa \bar{u}(z = \delta/k_0)}{u_*} = \left(\frac{u_{*1}}{u_*} \right)^3 \log \left(\frac{\delta}{k_1 z_\nu} \right) + G(X_0) - G(X_1), \quad (49)$$

with

$$G(X) = \left(\kappa c_\theta'' \frac{c_s}{u_{*s}} + 1 \right) X_0^{-6} [-X^4 - 2X^2 - 2 \log(1 - X^2)] \quad \text{and} \quad (50)$$

$$X_0 = \left(\frac{u_*}{2u_{*s}} \right)^{1/2}, \quad X_1 = \left(\frac{u_{*1}}{2u_{*s}} \right)^{1/2}. \quad (51)$$

The equivalent roughness z_0 is then found to be

$$z_0 = \frac{\delta}{k_0} \exp \left[- \frac{\kappa \bar{u}(z = \delta/k_0)}{u_*} \right] = \frac{\delta}{k_0} \left(\frac{\delta}{k_1 z_\nu} \right)^{-(u_{*1}/u_*)^3} \exp[-G(X_0) + G(X_1)] \quad (52)$$

and the Charnock coefficient becomes

$$\frac{z_0 g}{u_*^2} = \frac{\delta}{\alpha_2^2} \left(\frac{\delta}{k_1 z_\nu} \right)^{-(u_{*1}/u_*)^3} \exp[-G(X_0) + G(X_1)]. \quad (53)$$

This analytical expression allows us to examine how the Charnock coefficient depends on key nondimensional parameters, as described in the next subsection.

c. Discussion

First, note that the Charnock coefficient is proportional to

$$\left(\frac{\delta}{k_1 z_\nu} \right)^{-(u_{*1}/u_*)^3} = (10\delta \text{Re}_{*1})^{-(u_{*1}/u_*)^3}, \quad (54)$$

where $\text{Re}_{*1} = u_{*1}/\nu k_1$ is the friction Reynolds number of the flow over the smallest waves. Now, $(u_{*1}/u_*)^3$ varies depending on the degree of sheltering across the wave spectrum. When there is little sheltering, $u_{*1} \approx$

u_* and a large fraction of the total stress is supported by the viscous stress on the sea surface. Hence in this case, the Charnock coefficient varies inversely with Re_{*1} , as would be expected. But, when there is appreciable sheltering across the wave spectrum, $u_{*1} \ll u_*$ and

$$(10\delta \text{Re}_{*1})^{-(u_{*1}/u_*)^3} \rightarrow 1. \quad (55)$$

In this case the drag of the sea surface is dominated by the aerodynamic drag supported by the waves, and so there is no dependence on Reynolds number. In between these two asymptotic limits, the Charnock coefficient depends on Reynolds number with varying powers between 0 and -1 , depending on how much of the stress is supported by the waves. The estimates from Banner and Peirson (1998) show that $(u_{*1}/u_*)^3$ decreases roughly from 0.54 to 0.11 as the wind speed increases from 6 to 14 m s⁻¹ over mature seas. Therefore, we expect the Reynolds number dependence of the Charnock coefficient to reduce and become smaller at higher wind speeds.

Kitaigorodskii (1968) and others have argued that drag of the sea surface depends on the Reynolds number through processes similar to those acting in flow over a solid rough wall. Thus the flow is aerodynamically rough when $\text{Re}_\tau = u_* h_s / \nu \gg 1$ so that the roughness elements, of height h_s , are taller than the thickness of the depth of the viscous sublayer, of depth ν/u_* . Toba and Kunishi (1970) suggest that h_s should be taken to be the characteristic wave height, whereas Kitaigorodskii (1968) suggests that, since the roughness elements are the short waves, $h_s \sim 1$ cm. The implicit assumption in this picture is that the roughness elements act as bluff bodies inducing separated flow. The present model shows that this transition occurs differently when the surface is streamlined and the flow remains attached. It shows that large waves extract momentum from the wind (through pressure forces) so that shorter wavelength waves are “sheltered” and are exposed to a reduced stress. When sheltering is strong, the longer waves support the majority of the stress, leaving very little to be supported by surface viscous stress and hence little Reynolds number dependence.

Second, the Charnock coefficient also depends upon X_0 and X_1 , which are defined by

$$X_0^2 = \frac{u_*}{2u_{*s}} = \frac{1}{1 + (k_0/k_s)^{1/2}} \quad \text{and}$$

$$X_1^2 = \frac{u_{*1}}{2u_{*s}} = \frac{1}{1 + (k_1/k_s)^{1/2}}. \quad (56)$$

So X_0^2 and X_1^2 measure the extent of the equilibrium range, and the strength of sheltering in the equilibrium range that is, k_0 and k_1 and their relation to k_s . It is noteworthy that the Charnock coefficient depends on both.

When the sheltering is extremely strong, $k_1/k_s \rightarrow \infty$ so that $X_1^2 = u_{*1}/2u_{*s} \rightarrow 0$. In this limit $G(X_1) \rightarrow 0$. This limit is almost equivalent to the limit of $u_{*1}/u_* \rightarrow 0$ since $2u_{*s}/u_*$ is close to 1 (between 1.02 and 1.09 corresponding to the sheltering wavenumber c_s/u_{*s} between 0.46 and 2.38). Therefore, in this limit the Reynolds number dependence is also removed as discussed earlier. Then, the Charnock coefficient simplifies to

$$\frac{z_0 g}{u_*^2} = \frac{\delta}{\alpha_2^2} \exp[-G(X_0)], \quad (57)$$

with

$$G(X_0) = \left(\kappa c_\theta'' \frac{c_s}{u_{*s}} + 1 \right) \times X_0^{-6} [-X_0^4 - 2X_0^2 - 2 \log(1 - X_0^2)]. \quad (58)$$

The result is now a function of X_0 and c_s/u_{*s} . Since X_0 is uniquely related to the sheltering wave age, c_s/u_{*s} , through (26) and (27), the Charnock coefficient is a function of the sheltering wave age only. So, if the sheltering wave age is a true constant (i.e., independent of u_*), then the Charnock coefficient is also a true constant.

When, in practice, do we expect this simplified form (57) to be a good approximation? The limit $u_{*1}/u_* \rightarrow 0$ is valid when the majority of the stress is supported by form drag on the waves rather than by the surface viscous stress. In addition, this form has been obtained with an assumption that the analytical form of the equilibrium spectrum by Hara and Belcher (2002) is valid up to the cutoff wavenumber k_1 ; that is, that the effects of surface tension and viscous dissipation are small. Both conditions are expected to become increasingly valid as the wind speed increases.

In the atmospheric modeling community, the Charnock coefficient is commonly assumed to be a constant of about 0.010–0.015. However, the present model indicates that this assumption is strictly valid only if the following three conditions are satisfied:

- 1) The surface wave field is fully developed.
- 2) Effects of surface tension and viscosity are small, and the majority of the stress is supported by waves ($u_{*1}/u_* \rightarrow 0$).

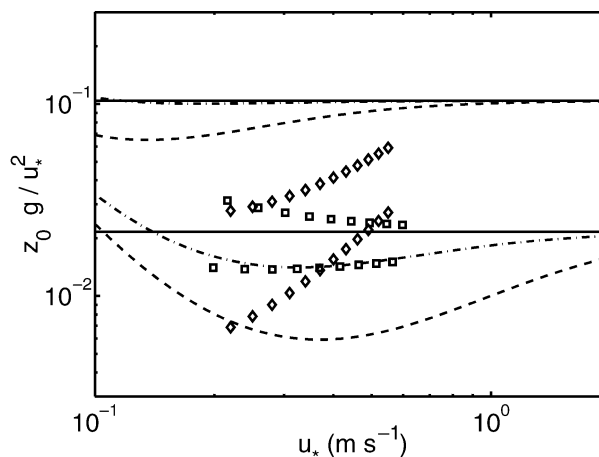


FIG. 4. Upper and lower bounds of the Charnock coefficient vs friction velocity for mature seas. Lines are results calculated with k_s estimated by approach II (dashed lines: $k_1 = 100 \text{ rad m}^{-1}$, dash-dot lines: $k_1 = 400 \text{ rad m}^{-1}$, and solid lines: asymptotic limit of $u_{*1}/u_* \rightarrow 0$), with sheltering wave age $c_s/u_{*s} = 0.46$ and 2.38. Diamonds are results calculated with k_s estimated by approach I. Squares are empirical estimates by Banner and Peirson (1998).

- 3) The sheltering wave age, c_s/u_{*s} , is a true constant, which, according to section 3, means that the equilibrium frequency/wavenumber spectrum is proportional to u_* not too far from the spectral peak.

Although the first two conditions are naturally expected, the validity of the third condition needs to be carefully examined in the future, by inspecting fully developed wave spectra under a wide range of wind forcing.

d. Calculation of the equivalent roughness over mature seas

The values of k_s and c_s/u_{*s} were determined for mature seas in the previous section. So, if $\delta = 0.05$ and when k_1 is specified, the Charnock coefficient can be calculated using (53). (In approach I, k_1 was set 100 rad m^{-1} ; in approach II k_1 is specified below.) Figure 4 shows the upper and lower bounds of the Charnock coefficient versus the friction velocity using the values of k_s presented in Fig. 1.

Let us first focus on the results calculated using k_s values estimated by approach II, shown by different lines. The upper and lower bounds correspond to the lower and upper bounds of k_s in Fig. 1 and the upper and lower bounds of c_s/u_{*s} in Fig. 2, respectively. For fixed u_* and k_1 , the Charnock coefficient varies by a factor of 5–10 depending on whether the upper bound or lower bound of c_s/u_{*s} is used. That is, the Charnock coefficient may significantly vary depending on the level of the equilibrium spectrum. The effect of choosing different k_1 (for a fixed c_s/u_{*s}) is also noteworthy. If k_1 is chosen to be above 400 rad m^{-1} , the calculated Charnock coefficient is not too far from the asymptotic limit (say, within a factor of 1.5).

We do not pursue here how the results are modified if spectral forms of gravity–capillary and capillary waves are introduced. However, the observation of the sensitivity of the results to different choices of k_1 suggests that knowledge of the spectral form at very large k is not critically important in determining the equivalent roughness at higher winds, particularly with larger values of the sheltering wave age c_s/u_{*s} .

So far, we have chosen a particular directionality of the growth rate $h(\theta) = \cos^2\theta$. If we choose a different form of $h(\theta)$, the result of the Charnock coefficient is modified through the change of c'_θ [by modifying the estimate of c_s/u_{*s} in (25)] and through the change of c''_θ [by modifying the coefficient in (50)]. Hara and Belcher (2002) show that c'_θ changes very little (from $3\pi/16 \cong 0.5890$ to $189\pi/1024 \cong 0.5798$) if $h(\theta)$ changes from $\cos^2\theta$ to $\cos^6\theta$. It is found that the coefficient c''_θ varies little also [from $16/(9\pi) \cong 0.5659$ to $32\,768/(19\,845\pi) \cong 0.5256$]. Therefore, our results of the Charnock coefficient are not sensitive to different choices of $h(\theta)$.

The Charnock coefficient is also calculated using k_s values estimated by approach I. The results, shown in Fig. 4 by diamonds, are within a factor of 2 or so of the empirical results by Banner and Peirson (1998), which are shown by squares. Since it is the drag that is usually required, which varies logarithmically with the Charnock coefficient, agreement within a factor of 2 is satisfying. The agreement found here is not obtained trivially: recall that approach I used only the empirical estimate of the relationship between the total stress and the surface viscous stress obtained by Banner and Peirson (1998); no information about the wind speed was used. Therefore, the combination of the present models for the equilibrium spectrum and the wave boundary layer produces the Charnock coefficient (or drag coefficient) that is consistent with the observations, provided that the relationship between the total stress and the surface viscous stress is given and reasonable values are set for the two parameters, α_2 and δ .

How do the present theoretical predictions compare to observations? The calculations have been completed here for mature wind seas, when the peak of the spectrum is beyond the region of wind forcing; that is, $u_*/c_p < \alpha_2 = 0.07$ (c_p is the phase speed at the spectral peak). It is therefore necessary to compare the results with observations that also satisfy this condition. Ebuchi and Toba (1991) report the Charnock coefficient of mature seas, with $u_*/c_p < 0.07$, spanning a wide range from 0.005 to 3. Later, Donelan et al. (1993) report values from 0.002 to 0.07, and mostly between 0.005 and 0.03. Johnson et al. (1998) present values between 0.002 and 0.2, and mostly between 0.005 and 0.04. The more recent study of Drennan et al. (2003), which carefully selected only pure wind-sea conditions, show values between 0.005 and 0.1, and mostly between 0.005 and 0.05. They also show that most of previously proposed empirical parameterizations fall roughly between

0.007 and 0.05. The value from the present model ranges from 0.02 to 0.1, which has a strong overlap with values observed by Drennan et al. (2003).

The asymptotic analysis shows that the Charnock coefficient becomes a constant at very high winds only. However, Fig. 3 shows that in practice the Charnock coefficient varies by at most a factor of 2 through all wind speeds provided the sheltering wave age is constant and k_1 is chosen to be above 400 rad m^{-1} . Therefore, it seems to be reasonable, in practice, to use a constant Charnock coefficient over mature seas at all wind speeds. This finding, however, does not mean that the original dimensional argument by Charnock (1955), that the only g and u_* are relevant external parameters to determine the roughness length, is valid at lower winds. The Charnock coefficient does depend on the Reynolds number significantly at lower winds. (For example, if we change the value of air viscosity significantly, the Charnock coefficient will not remain constant!)

The results of the Charnock coefficient obtained using the same wave spectrum but different wave boundary layer models based on various forms of the eddy viscosity (Janssen 1989; Chalikov and Makin 1991; Makin et al. 1995; Makin and Kudryavtsev 1999) are discussed in appendix C.

e. Determination of the wind profile in the wave boundary layer

In section 4d, it was shown that the mean wind speed at the top of the wave boundary layer (and hence the Charnock coefficient) is uniquely determined from the conservation of momentum and energy inside the wave boundary layer, provided the viscous dissipation of the TKE is related to the local, reduced turbulent stress at each height. In order to determine the vertical wind profile inside the wave boundary layer, two further conditions need to be introduced.

First, linear analyses of airflow over sinusoidal waves (Belcher and Hunt 1993; Belcher 1999) show that the vertical decay of the pressure transport $-\overline{w\overline{p}}$ associated with a particular wavenumber k decays vertically over the same length scale as the wave-induced stress. Hence, the vertical variation of $-\overline{w\overline{p}}$ is represented here by the same function as for the wave-induced stress, namely $F(k, z)$ defined in (4). Then, we may write

$$\Pi(z) = \int_0^\infty \tilde{F}_w(k)F(k, z) dk = \int_0^{\delta/z} \tilde{F}_w(k) dk, \quad (59)$$

so that the vertical gradient of Π is

$$\frac{d\Pi(z)}{dz} = \frac{d}{dz}\left(\frac{\delta}{z}\right)\tilde{F}_w\left(k = \frac{\delta}{z}\right) = -\frac{\delta}{z^2}\tilde{F}_w\left(k = \frac{\delta}{z}\right). \quad (60)$$

Second, we suppose that within the wave boundary layer

the divergence of the turbulent transport $d\Pi'/dz$ is smaller than the other terms in the energy balance, as it is in a homogeneous rough-wall boundary layer.

Introducing (44) and (60) into (38) and setting $d\Pi'/dz = 0$, the net energy budget then becomes

$$\frac{d}{dz}(\bar{u}\tau_{\text{tot}}) - \frac{\delta}{z^2}\tilde{F}_w\left(k = \frac{\delta}{z}\right) - \rho_a \frac{[u_*^l(k = \delta/z)]^3}{\kappa z} = 0. \tag{61}$$

This energy conservation equation, evaluated at each height, may be used to determine the wind profile inside the wave boundary layer. [Compare this with the integrated energy budget (43) that was used in section 4d.]

Introducing (45) into (61), the vertical gradient of wind speed is expressed as

$$\frac{d\bar{u}}{dz} = \frac{u_*}{\kappa z}, \quad \frac{\delta}{k_0} < z, \tag{62}$$

$$\frac{d\bar{u}}{dz} = \frac{u_*}{\kappa z} \left(\kappa c_\theta'' \frac{c_s}{u_{*s}} + 1 \right) \times \left[\frac{u_*^l(k = \delta/z)}{u_*} \right]^3, \quad \frac{\delta}{k_1} < z < \frac{\delta}{k_0}, \tag{63}$$

and

$$\frac{d\bar{u}}{dz} = \frac{u_*}{\kappa z} \left(\frac{u_{*1}}{u_*} \right)^3, \quad z_v < z < \frac{\delta}{k_1}. \tag{64}$$

On integrating (62)–(64) in z , we may write the mean wind speed analytically as (see appendix B for the derivation)

$$\bar{u}(z) = \frac{u_*}{\kappa} \left(\frac{u_{*1}}{u_*} \right)^3 \log\left(\frac{z}{z_v}\right), \quad z_v \leq z < \frac{\delta}{k_1}, \tag{65}$$

$$\bar{u}(z) = \frac{u_*}{\kappa} \left[\left(\frac{u_{*1}}{u_*} \right)^3 \log\left(\frac{\delta}{k_1 z_v}\right) + G(X) - G(X_1) \right], \quad \frac{\delta}{k_1} \leq z < \frac{\delta}{k_0}, \quad \text{and} \tag{66}$$

$$\bar{u}(z) = \frac{u_*}{\kappa} \left[\left(\frac{u_{*1}}{u_*} \right)^3 \log\left(\frac{\delta}{k_1 z_v}\right) + G(X_0) - G(X_1) + \log\left(\frac{k_0 z}{\delta}\right) \right], \quad \frac{\delta}{k_0} \leq z, \tag{67}$$

with

$$G(X) = \left(\kappa c_\theta'' \frac{c_s}{u_{*s}} + 1 \right) \times X_0^{-6} [-X^4 - 2X^2 - 2 \log(1 - X^2)] \tag{68}$$

and

$$X = \left[\frac{u_*^l(k = \delta/z)}{2u_{*s}} \right]^{1/2}, \quad X_0 = \left(\frac{u_*}{2u_{*s}} \right)^{1/2}, \quad \text{and} \tag{69}$$

$$X_1 = \left(\frac{u_{*1}}{2u_{*s}} \right)^{1/2}.$$

In the asymptotic limit of $u_{*1}/u_* \rightarrow 0$, the wind profile becomes

$$\bar{u}(z) = \frac{u_*}{\kappa} G(X), \quad 0 \leq z < \frac{\delta}{k_0}, \tag{70}$$

and

$$\bar{u}(z) = \frac{u_*}{\kappa} \left[G(X_0) + \log\left(\frac{k_0 z}{\delta}\right) \right], \quad \frac{\delta}{k_0} \leq z. \tag{71}$$

In Fig. 5 the mean wind profiles are shown with the friction velocity $u_* = 0.5 \text{ m s}^{-1}$, the sheltering wave age

$c_s/u_{*s} = 0.46$, and different choices of k_1 . Just below the top of the wave boundary layer ($z = \delta/k_0$, indicated by diamonds), the wind profile becomes slightly steeper because the loss of the kinetic energy of the mean flow is enhanced by the energy flux into surface waves. How-

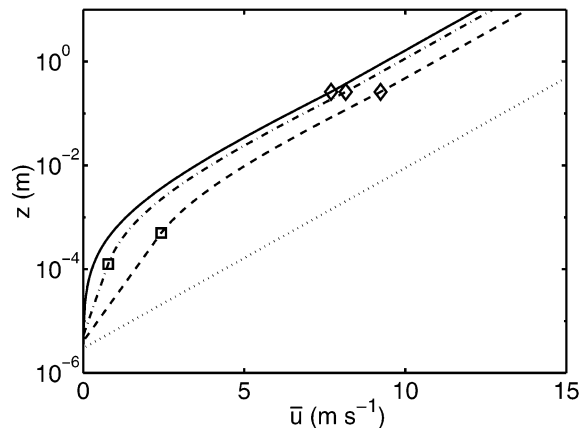


FIG. 5. Mean wind profiles over mature seas. Friction velocity $u_* = 0.5 \text{ m s}^{-1}$. Sheltering wave age $c_s/u_{*s} = 0.46$. Dashed line: $k_1 = 100 \text{ rad m}^{-1}$, dash-dot line: $k_1 = 400 \text{ rad m}^{-1}$, and solid line: asymptotic limit of $u_{*1}/u_* \rightarrow 0$. Diamonds ($z = \delta/k_0$) and squares ($z = \delta/k_1$) indicate top and bottom of the wave boundary layer, respectively. Dotted line shows wind profile over a smooth solid surface.

ever, the slope of the wind profile rapidly decreases toward the bottom of the wave boundary layer ($z = \delta/k_1$, indicated by squares) because the viscous dissipation of the TKE is reduced corresponding to the reduction of the turbulent stress τ_t . The asymptotic result (solid line) is a reasonable approximation for $k_1 \geq 400 \text{ rad m}^{-1}$.

The wave boundary layer model presented here yields the expression for the eddy viscosity K inside the wave boundary layer. (In contrast, previous models needed to specify the eddy viscosity.) Define the eddy viscosity such that

$$\frac{\tau_t(z)}{\rho_a} = \left[u_*^i \left(k = \frac{\delta}{z} \right) \right]^2 = K \frac{d\bar{u}}{dz}. \quad (72)$$

Then, from (63), we obtain

$$K = \kappa u_* z \left(\kappa c_0'' \frac{c_s}{u_{*s}} + 1 \right)^{-1} \left[\frac{u_*^i(k = \delta/z)}{u_*} \right]^{-1}, \quad (73)$$

$$\frac{\delta}{k_1} < z < \frac{\delta}{k_0}.$$

The eddy viscosity is affected by surface waves in two different ways. The first bracket on the right decreases the eddy viscosity by a fixed factor throughout the wave boundary layer. The second bracket on the right illustrates the effect of sheltering on the eddy viscosity, which is small near the top of the wave boundary layer but increases toward the bottom of the wave boundary layer where the turbulent stress is reduced.

5. Concluding remarks

We have developed a model of the wave boundary layer based on the conservation of momentum and energy. Energy conservation was cast as a bulk constraint, integrated across the depth of the wave boundary layer. The turbulence closure was then achieved by parameterizing the viscous dissipation rate of the TKE, ε , in terms of the local turbulent stress τ_t , following what is done in conventional one-equation models of turbulence. Momentum conservation was accounted for using the analytical model of the equilibrium surface wave spectra developed by Hara and Belcher (2002). This allowed us to obtain analytical expressions for the Charnock coefficient and to examine the results in terms of key non-dimensional parameters. The results are generally consistent with previous observations and existing empirical parameterizations of the Charnock coefficient.

The strength of the analytical model developed here is that we have been able to identify the conditions for the Charnock coefficient to be a true constant. They are (i) the surface wave field is fully developed, (ii) the effects of surface tension and viscosity are small and most of the stress is supported by the wave drag, and (iii) the sheltering wave age is independent of wind stress; that is, the frequency/wavenumber spectrum not too far from the peak is proportional to the wind friction velocity.

One fundamental question that arises from this study is whether the sheltering wave age (c_s/u_{*s}) is truly independent of wind stress. The sheltering wave age should be constant if the frequency/wavenumber spectrum not too far from the peak is proportional to the friction velocity. A constant sheltering wave age is also a necessary requirement for the Charnock coefficient to be a true constant over mature seas. Field observations of equilibrium wave spectra under wide ranges of wind forcing are needed to answer this question.

When the wind sea is growing, the wave spectrum near the peak is clearly outside the equilibrium range, but contributes to the wave-induced stress. Hence the present model based on the equilibrium spectral model is not complete. If, however, the wave spectrum near the peak is known (either through observations or through numerical simulations) and the tail part of the spectrum is specified using the equilibrium spectral model, the wind profile and the drag coefficient may be calculated using the present wave boundary layer model. This may be a reasonable next step to examine the drag coefficient over growing and confused seas.

Last, as suggested by Makin and Kudryavtsev (2002), breaking waves may significantly enhance the roughness length. How might the present model be affected by breaking waves? Bulk energy conservation, as schematically shown in Fig. 3, always needs to be satisfied. Breaking waves are likely to modify the total energy flux into surface waves and the viscous dissipation inside the wave boundary layer. At present it is difficult to quantify these effects since our knowledge of breaking wave processes, such as statistical distribution of breaking waves and energy and momentum flux into individual breaking waves, is poor with uncertainties of factor of 10 or larger.

Although we cannot present quantitative arguments that neglecting breaking wave effects does not change appreciably our model results, the model shows, for the first time, a simple analytical picture of how the Charnock coefficient depends on different parameters and it yields the necessary conditions for the Charnock coefficient to be a true constant. This model framework will be a reasonable starting point to investigate breaking wave effects once our quantitative estimates of breaking wave processes become sufficiently constrained.

Acknowledgments. We thank the U.S. Office of Naval Research (CBLAST program, Grants N00014-0110125 and N00014-0110133) for supporting this research. Author TH also thanks the U.S. National Science Foundation (Grant OCE0002314) for additional support.

APPENDIX A

Nonconservation of Energy in the Wave Boundary Layer

In past studies, two eddy viscosity models were proposed to determine the wind profile over surface waves.

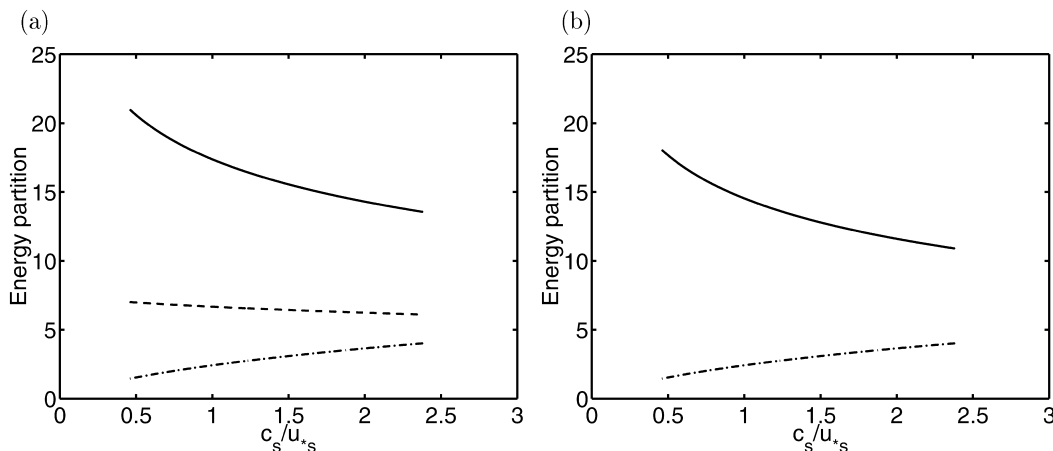


FIG. A1. Partition of the energy flux from the top of the wave boundary layer into the internal dissipation and the flux into surface waves. Results are shown vs sheltering wave age. Solid line: $F_T/\rho_a u_*^3$, dashed line: $(F_T - F_D)/\rho_a u_*^3$, and dash-dot line: $F_B/\rho_a u_*^3$. (a) Results with the first eddy viscosity model (Janssen 1989; Chalikov and Makin 1991; Makin et al. 1995); (b) results with the second eddy viscosity model (Makin and Kudryavtsev 1999).

Here, we consider the energy budget inside the wave boundary layer using the two eddy viscosity models. With both models, the mean wind profile inside the wave boundary layer is related to the turbulent stress as

$$\frac{\tau_i(z)}{\rho_a} = \left[u_*' \left(k = \frac{\delta}{z} \right) \right]^2 = K \frac{d\bar{u}}{dz}, \quad (\text{A1})$$

where K is the eddy viscosity and the viscous dissipation rate is scaled as

$$\varepsilon = K^3 (\kappa z)^{-4}. \quad (\text{A2})$$

The first eddy viscosity model, used by Janssen (1989), Chalikov and Makin (1991), and Makin et al. (1995), is simply related to the turbulent stress; that is,

$$K = \kappa u_*' (k = \delta/z) z. \quad (\text{A3})$$

The second eddy viscosity parameterization, proposed by Makin and Kudryavtsev (1999), was obtained from the TKE budget. It was assumed that the main balance was between the shear production $\tau_{\text{tot}} d\bar{u}/dz$ and the viscous dissipation $\rho_a \varepsilon$. Then, the eddy viscosity parameterization is expressed as

$$K = \kappa u_* z \left[\frac{u_*' (k = \delta/z)}{u_*} \right]^{1/2}. \quad (\text{A4})$$

If we introduce (45), (A1), (A2), and the first eddy viscosity model (A3) into the energy equation

$$\frac{d}{dz} (\bar{u} \tau_{\text{tot}}) - \frac{\delta}{z^2} \tilde{F}_w \left(k = \frac{\delta}{z} \right) - \rho_a \varepsilon = 0 \quad (\text{A5})$$

derived in section 4d, we obtain

$$\begin{aligned} & \frac{\rho_a u_*^3}{\kappa z} \frac{u_*' (k = \delta/z)}{u_*} - \frac{\rho_a u_*^3}{z} c_\theta'' \frac{c_s}{u_*} \left[\frac{u_*' (k = \delta/z)}{u_*} \right]^3 \\ & - \frac{\rho_a u_*^3}{\kappa z} \left[\frac{u_*' (k = \delta/z)}{u_*} \right]^3 = 0. \end{aligned} \quad (\text{A6})$$

Let us examine the overall energy budget inside the wave boundary layer over mature seas. We consider the asymptotic limit of $u_{*1}/u_* \rightarrow 0$ and integrate the three terms in (A6) from $z = 0$ to $z = \delta/k_0$. The results are written analytically (see appendix B for derivation) as

$$\frac{F_T}{\rho_a u_*^3} = \frac{1}{\kappa} (-2X_0^{-2}) \log(1 - X_0^2), \quad (\text{A7})$$

$$\frac{F_B}{\rho_a u_*^3} = c_\theta'' \frac{c_s}{u_*} X_0^{-6} [-X_0^4 - 2X_0^2 - 2 \log(1 - X_0^2)], \quad (\text{A8})$$

and

$$\frac{F_D}{\rho_a u_*^3} = \frac{1}{\kappa} X_0^{-6} [-X_0^4 - 2X_0^2 - 2 \log(1 - X_0^2)]. \quad (\text{A9})$$

Here, F_T , F_B , and F_D denote the integral of the first, second, and third terms, respectively. For a given sheltering wave age (i.e., for a given X_0), we may compare the magnitude of these three quantities. In Fig. A1a we present how the total energy flux from the top of the wave boundary layer (F_T) is partitioned into the internal dissipation (F_D) and the flux into surface waves (F_B). All the results are normalized by $\rho_a u_*^3$ and are presented versus the sheltering wave age c_s/\bar{u}_s between 0.46 and 2.38. Here, the solid line is the total flux from the top ($F_T/\rho_a u_*^3$), the dashed line is the total excess energy, that is, the total flux from the top minus the internal dissipation $[(F_T - F_D)/\rho_a u_*^3]$, and the dash-dot line is the flux into surface waves at the bottom of the wave bound-

ary layer ($F_B/\rho_a u_*^3$). The energy is conserved if the dashed line and the dash-dot line overlap. Clearly, the eddy viscosity model (A3) underestimates the viscous dissipation and/or overestimates the shear production.

If we introduce (A1), (A2), and the second eddy viscosity model (A4) into the energy equation and integrate it from $z = 0$ to $z = \delta/k_0$, the results are written as

$$\frac{F_T}{\rho_a u_*^3} = \frac{F_D}{\rho_a u_*^3} = \frac{1}{\kappa} X_0^{-3} \left[-4X_0 + 2 \log \left(\frac{1 + X_0}{1 - X_0} \right) \right], \quad (\text{A10})$$

and $F_B/\rho_a u_*^3$ is the same as (A8). We find that F_T and F_D exactly cancel out as expected. In Fig. A1b we present the total flux from the top ($F_T/\rho_a u_*^3$) with the solid line and the flux into surface waves at the bottom of the wave boundary layer ($F_B/\rho_a u_*^3$) with the dash-dot line. The total excess energy {the total flux from the top minus the internal dissipation [$(F_T - F_D)/\rho_a u_*^3$]} is zero; that is, there is no energy left for surface waves. Therefore, the second eddy viscosity model (A4) overestimates the viscous dissipation and/or underestimates the shear production.

APPENDIX B

Evaluation of the Integral of the Local Friction Velocity

Let us evaluate the following integral of the local friction velocity,

$$\int_{\delta/k_1}^{\delta/k} \left[\frac{u_*^l(k = \delta/z)}{u_*} \right]^n \frac{dz}{z} = \int_k^{k_1} \left[\frac{u_*^l(k')}{u_*} \right]^n \frac{dk'}{k'}, \quad (\text{B1})$$

which can be written

$$\begin{aligned} & \left(\frac{2u_{*s}}{u_*} \right)^n \int_{\delta/k_1}^{\delta/k} \left[1 + \left(\frac{\delta}{k_s z} \right)^{1/2} \right]^{-n} \frac{dz}{z} \\ &= \left(\frac{2u_{*s}}{u_*} \right)^n \int_k^{k_1} \left[1 + \left(\frac{k'}{k_s} \right)^{1/2} \right]^{-n} \frac{dk'}{k'}. \end{aligned} \quad (\text{B2})$$

We introduce a variable X' such that

$$X'^2 = \frac{u_*^l(k')}{2u_{*s}} = \left[1 + \left(\frac{k'}{k_s} \right)^{1/2} \right]^{-1} \quad \text{and} \quad (\text{B3})$$

$$\frac{dk'}{k'} = \frac{-4}{X'(1 - X'^2)} dX'. \quad (\text{B4})$$

Then, (B2) can be written

$$\begin{aligned} & \left(\frac{2u_{*s}}{u_*} \right)^n \int_k^{k_1} \left[1 + \left(\frac{k'}{k_s} \right)^{1/2} \right]^{-n} \frac{dk'}{k'} \\ &= X_0^{-2n} \int_{X_1}^X \frac{4X'^{2n}}{X'(1 - X'^2)} dX' \end{aligned} \quad (\text{B5})$$

with

$$\begin{aligned} X &= \left[\frac{u_*^l(k = \delta/z)}{2u_{*s}} \right]^{1/2}, \quad X_0 = \left(\frac{u_*}{2u_{*s}} \right)^{1/2}, \quad \text{and} \\ X_1 &= \left(\frac{u_{*1}}{2u_{*s}} \right)^{1/2}. \end{aligned} \quad (\text{B6})$$

The integral on the right of (B5) may be solved analytically as

$$\int_{X_1}^X \frac{4X'}{1 - X'^2} dX' = [-2 \log(1 - X'^2)]_{X_1}^X \quad (\text{B7})$$

for $n = 1$,

$$\int_{X_1}^X \frac{4X'^2}{1 - X'^2} dX' = \left[-4X' + 2 \log \left(\frac{1 + X'}{1 - X'} \right) \right]_{X_1}^X \quad (\text{B8})$$

for $n = 3/2$, and

$$\begin{aligned} & \int_{X_1}^X \frac{4X'^5}{1 - X'^2} dX' \\ &= [-X'^4 - 2X'^2 - 2 \log(1 - X'^2)]_{X_1}^X \end{aligned} \quad (\text{B9})$$

for $n = 3$.

APPENDIX C

Charnock Coefficient with Different Eddy Viscosity Models

Let us calculate the Charnock coefficient over mature seas (idealized model) using the same equilibrium wave spectrum but two eddy viscosity models discussed in appendix A:

$$\frac{d\bar{u}}{dz} = \frac{[u_*^l(k = \delta/z)]^2}{K} = \frac{u_*}{\kappa z} \left[\frac{u_*^l(k = \delta/z)}{u_*} \right]^n, \quad (\text{C1})$$

with $n = 1$ (Janssen 1989; Chalikov and Makin 1991; Makin et al. 1995) and $n = 3/2$ (Makin and Kudryavtsev 1999). The results can be expressed analytically as (see appendix B for derivation)

$$\frac{z_0 g}{u_*^2} = \frac{\delta}{\alpha_2^2 (k_1 z_v)} \exp[-G_n(X_0) + G_n(X_1)] \quad (\text{C2})$$

with

$$G_1(X) = X_0^{-2} [-2 \log(1 - X^2)] \quad (\text{C3})$$

for $n = 1$ and

$$G_{3/2}(X) = X_0^{-3} \left[-4X + 2 \log \left(\frac{1 + X}{1 - X} \right) \right] \quad (\text{C4})$$

for $n = 3/2$. The asymptotic results of $u_{*1}/u_* \rightarrow 0$ are

$$\frac{z_0 g}{u_*^2} = \frac{\delta}{\alpha_2^2} (1 - X_0^2)^{2X_0^2} \quad (\text{C5})$$

for $n = 1$ and

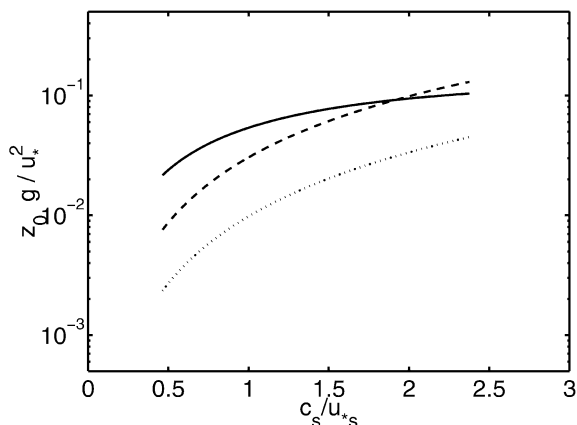


FIG. C1. Charnock coefficient vs the sheltering wave age c_s/u_{*s} for mature seas. Asymptotic results of $u_{*s}/u_* \rightarrow 0$. Dotted lines: eddy viscosity model with $n = 1$ (Janssen 1989; Chalikov and Makin 1991; Makin et al. 1995), dashed lines: eddy viscosity model with $n = 2/3$ (Makin and Kudryavtsev 1999), and solid lines: the present model.

$$\frac{z_0 g}{u_*^2} = \frac{\delta}{\alpha_*^2} \left(\frac{1 + X_0}{1 - X_0} \right)^{-2X_0^{-3}} \exp(4X_0^{-2}) \quad (\text{C6})$$

for $n = 3/2$. These asymptotic results are shown in Fig. C1 and compared with the results of this study. The eddy viscosity model with $n = 1$ yields lower values of the Charnock coefficient than the other two models. The difference between the eddy viscosity model with $n = 3/2$ and the present model is small at larger sheltering wave age but the former yields a lower value at lower sheltering wave age. Therefore, the present model results are less sensitive to the choice of the sheltering wave age values, that is, less sensitive to the level of the equilibrium spectrum.

REFERENCES

- Banner, M. L., and W. L. Peirson, 1998: Tangential stress beneath wind-driven air–water interfaces. *J. Fluid Mech.*, **364**, 115–145.
- Belcher, S. E., 1999: Wave growth by non-separated sheltering. *Eur. J. Mech. B/Fluids*, **18**, 447–462.
- , and J. C. R. Hunt, 1993: Turbulent shear flow over slowly moving waves. *J. Fluid Mech.*, **251**, 109–148.
- Chalikov, D., and V. Makin, 1991: Models of the wave boundary layer. *Bound.-Layer Meteor.*, **56**, 83–99.
- Charnock, H., 1955: Wind stress on a water surface. *Quart. J. Roy. Meteor. Soc.*, **81**, 639–640.
- Donelan, M. A., F. W. Dobson, S. D. Smith, and R. J. Anderson, 1993: On the dependence of sea surface roughness on wave development. *J. Phys. Oceanogr.*, **23**, 2143–2149.
- , W. M. Drennan, and K. Katsaros, 1997: The air–sea momentum flux in conditions of wind sea and swell. *J. Phys. Oceanogr.*, **27**, 2087–2099.
- Drennan, W. M., H. C. Graber, D. Hauser, and C. Quentin, 2003: On the wave age dependence of wind stress over pure wind seas. *J. Geophys. Res.*, **108**, 8062, doi:10.1029/2000JC000715.
- Ebuchi, N., and Y. Toba, 1991: Sea-surface roughness length fluctuating in concert with wind and waves. *J. Oceanogr. Soc. Japan*, **47**, 63–79.
- Hara, T., and S. E. Belcher, 2002: Wind forcing in the equilibrium range of wind-wave spectra. *J. Fluid Mech.*, **470**, 223–245.
- Janssen, P. A. E. M., 1989: Wave-induced stress and the drag of air flow over sea waves. *J. Phys. Oceanogr.*, **19**, 745–754.
- Johnson, H. K., J. Hjstrup, H. J. Vested, and S. E. Larsen, 1998: On the dependence of sea surface roughness on wind waves. *J. Phys. Oceanogr.*, **28**, 1702–1716.
- Jones, I. S. F., and Y. Toba, 2001: *Wind Stress over the Ocean*. Cambridge University Press, 307 pp.
- Kitaigorodskii, S. A., 1968: On the calculation of the aerodynamic roughness of the sea surface. *Izv. Atmos. Oceanic Phys.*, **4**, 870–878.
- Kudryavtsev, V. N., and V. K. Makin, 2001: The impact of air-flow separation on the drag of the sea surface. *Bound.-Layer Meteor.*, **98**, 155–171.
- , —, and B. Chapron, 1999: Coupled sea surface–atmosphere model. 2. Spectrum of short wind waves. *J. Geophys. Res.*, **104**, 7625–7639.
- Makin, V. K., and C. Mastenbroek, 1996: Impact of waves on air–sea exchange of sensible heat and momentum. *Bound.-Layer Meteor.*, **79**, 279–300.
- , and V. N. Kudryavtsev, 1999: Coupled sea surface–atmosphere model. 1. Wind over waves coupling. *J. Geophys. Res.*, **104**, 7613–7623.
- , and —, 2002: Impact of dominant waves on sea drag. *Bound.-Layer Meteor.*, **103**, 83–99.
- , —, and C. Mastenbroek, 1995: Drag of the sea surface. *Bound.-Layer Meteor.*, **73**, 159–182.
- Mason, P. J., 1988: The formation of areally-averaged roughness lengths. *Quart. J. Roy. Meteor. Soc.*, **114**, 399–420.
- Phillips, O. M., 1977: *The Dynamics of the Upper Ocean*. 2d ed. Cambridge University Press, 336 pp.
- , 1985: Spectral and statistical properties of the equilibrium range in wind-generated gravity waves. *J. Fluid Mech.*, **156**, 505–531.
- Plant, W. J., 1982: A relationship between wind stress and wave slope. *J. Geophys. Res.*, **87**, 1961–1967.
- Taylor, P. K., and M. J. Yelland, 2001: The dependence of sea surface roughness on the height and steepness of the waves. *J. Phys. Oceanogr.*, **31**, 572–590.
- Toba, Y., and H. Kunishi, 1970: Breaking of wind waves and the sea surface wind stress. *J. Oceanogr. Soc. Japan*, **26**, 71–80.
- Yelland, M., and P. K. Taylor, 1996: Wind stress measurements from the open ocean. *J. Phys. Oceanogr.*, **26**, 541–558.